

# Memoryless radial basis function neural network based proportional integral controller for PMSM drives

Md. Alamgir Hossain, Md. Shahjahan

Department of Electrical and Electronic Engineering, Khulna University of Engineering and Technology, Khulna, Bangladesh

## Article Info

### Article history:

Received Jul 25, 2022

Revised Nov 1, 2022

Accepted Nov 13, 2022

### Keywords:

Neural network  
PMSM drive  
RBFNN  
Speed controller  
Vector control

## ABSTRACT

This research paper presents the memoryless radial basis function neural network (RBFNN) dependent proportional integral (PI) controller for permanent magnet synchronous motor (PMSM) drives. The proposed RBFNN is memoryless adaptation scheme since the algorithm neither use the past samples nor retain the previous adaptation direction and hence the observations are used only once. Firstly, mathematical model for PMSM drive is explained and then structure of RBFNN controller is formulated. RBFNN consists of single input, a hidden layer with five neurons, a single output layer that are used to track the speed of the machine. The Jacobian matrix obtained from RBFNN is used to adjust the gain of the speed and applied to PI controller. The performance of the PI based vector controller with and without RBFNN are compared through the simulation by using MATLAB/Simulink environment. The simulations show that the proposed RBFNN outperform the existing PI based control method and enhances the speed tracking of PMSM drives.

This is an open access article under the [CC BY-SA](https://creativecommons.org/licenses/by-sa/4.0/) license.



## Corresponding Author:

Md. Alamgir Hossain

Department of Electrical and Electronic Engineering, Khulna University of Engineering and Technology

Khulna-9203, Bangladesh

Email: mah@eee.kuet.ac.bd

## 1. INTRODUCTION

Permanent magnet synchronous motors (PMSM) drives became one of the vital components for large-scale industrial automation, wind power generation, and autonomous vehicles. due to its compact size, high power to weight ratio, large torque to inertia ratio, maintenance-free feature as well as the advancement of power electronics based control strategy [1]-[3]. Besides, compared to the induction machine PMSM has the high efficiency due to absence of rotor loss [4]. However, PMSM itself is non-linear multi-variable system and the performance of this machine suffers due to variations of parameter and hence the control system is affected. So, design a high-efficient, fast responsive, and robust controller against the motor parameter fluctuations is the key research area of the researchers around the globe. A typical PMSM machine has a three phase stator and rotor having surface mounted magnets (surface-PMSM) or magnet inside the rotor body (interior PMSM), and an interior-PMSM is shown in Figure 1. But, the unpredictable machine parameter, for example non-linear dynamic and outer load interference of PMSM degrade the performance of this drive and PMSM became the key research area of the academician and researchers. The conventional proportional integral (PI), proportional integral derivative (PID), and adaptive PID controller for electric motor control have numerous applications in industrial process due to its simplicity and easy to implement [5]-[8] and still popular in actual PMSM system. But, this controller is only applicable for linear system model from where the system parameters may be obtained easily. Though, the conventional PID control method attracted the controller market for PMSM

for the simplicity, but this strategy is not suitable to encounter the external torque variation and structural perturbations during the operation. Various methods have been listed in the literature so far to mitigate these limitations of the drives to swap PID controller.

Hence, depending upon the characteristics model of PMSM, various new control methods has been addressed in the research literature. A non-linear and the sliding mode of control [9]-[14] have been investigated to address the position and controlling the speed of PMSM. Due to robustness to external load variations and fast response to dynamic system, the sliding mode control (SMC) has been gaining the scope in speed control of PMSM drives. But, this method still is affected by the parameter variation as well as chattering issues. In the literature, researchers have proposed different model predictive control (MPC) [15]-[19] based on various model parameter estimation algorithms. The MPC control method is entirely dependent on the known/estimated parameter from the model, and this unknown parameters are estimated with the help of suitable algorithm that results calculation complexity and uncertainty. In [15], overmodulation is used and the major limitations of the overmodulation are harmonic current insertion to the system and smooth transfer of control region from linear to overmodulation region. The adaptive  $H_\infty$  controller has been exploited for the control of PMSM in [20]. In addition to nonlinear control and methods stated above different artificial intelligent speed control methods are also available. For example, the artificial intelligence based expert system, fuzzy logic controller as well as neural networks [21], [22] have been also applied in drive systems. To regulate the gain of a controller, Brock *et al.* [23] used fuzzy logic system based sliding mode control of speed and position for PMSM drives. Nonetheless, there are some controller parameters consisting uncertainty and can be adjusted empirically that will consume more time and may not be optimal for constant error with different speed conditions.

Radial basis function neural network (RBFNN) is one of various neural network methods that has been studied thoroughly and applied to control many drive systems in recent year [24]-[26]. RBFNN evinces its innate characteristics of simple architecture, fast learning rate, and have better approximation abilities. But, a few attention is exerted to control the speed of PMSM by using this robust neural network algorithm [27], [28] and hence an in depth research is required to exploit the feature of RBFNN. From this inspiration, a memoryless RBFNN speed control method for PMSM is developed in this paper.

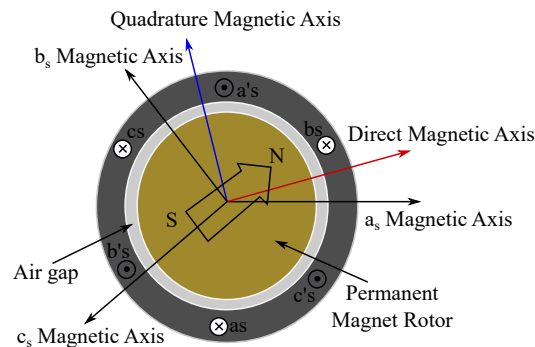


Figure 1. Field orientation of PMSM

This research paper is structured in section-wise order: dynamic mathematical system model of PMSM and conventional vector control strategy are discussed in second section. In section 3, the structure of RBFNN is thoroughly explained by exploiting the functional block diagram. Section four is based on simulation results and discussion, and the conclusion is addressed in the last section.

## 2. DYNAMIC SYSTEM MODEL OF PMSM

PMSM is one kind of synchronous machine without the need of DC supply for its excitation. Instead, permanent magnet in rotor supplies required excitation or field flux that concentrates to only one axis. The machine model used in this research is a three phase motor, hence it has three phase windings inside the stator only and the permanent magnets mounted in the rotor. As stated, regular synchronous motor needs both AC and DC supplies for its operation, but PMSM requires only AC and it is one of the greatest advantages for the

preference of PMSM. The dynamic model obtained in stator frame is inappropriate as the stator inductances are the function of rotor position. So, the PMSM dynamic model can be derived by using only one set of two stator windings with the help of dq axes principle. Hence, for proper analysis, stator windings of constant inductances are the primary concern, and this can be obtained by using generalized winding transformation theory. In this case, a fictitious set of dq windings are introduced in the rotor that rotates at the electrical speed of the rotor. Clearly, the inductance of these dq windings will be constant as these rotate with the same speed of the rotor. Based on observation and using the graphical projection, these two-phase model will be used to derive three-phase machine model with the help of transformation, and this is possible to extend the model to an n-phase machine. The three-phase machine parameters, i.e. voltage, currents, and flux linkage will be derived with the help of two-phase quantities.

The differential equations of PMSM are nonlinear. Normally the drive system might have the variables of DC quantities to use the hidden feature of linear control methodology for stability analysis and controller design, but actual quantities are sinusoidal though. Therefore, the system is linearized by perturbing the equations of the machine with a steady-state point and the resulting equations are small-signal system of equations. These type of small-signal system can be obtained with the help of reference axes rotating the synchronous speed. As the reference speed is similar to the sinusoidal supply angular speed, the difference in speed among them will be zero. So, sinusoid will be act as a DC signal with respect to reference frame. Now, it will be easy to deduce a small-signal equations excluding the nonlinear equations around the operating point that is described by only DC value. The three-phase stator currents are given by:

$$i_{as} = i_s \sin(\omega_r t + \delta) \quad (1)$$

$$i_{bs} = i_s \sin(\omega_r t + \delta - \frac{2\pi}{3}) \quad (2)$$

$$i_{cs} = i_s \sin(\omega_r t + \delta + \frac{2\pi}{3}) \quad (3)$$

where,  $\delta$  is the torque angle, and the rotor as well as its field travel at the speed of  $\omega_r$  electrical radian/second. The stator currents in q-axis and d-axis into rotor reference are received by using the proper transformation method. Assume that the turns number,  $N_1$  and current magnitude are equal of every 3-phases. Then for the sake of equal mmf, for two-phase system the number of turns per phase will be  $3N_1/2$ . The mmfs of q- and d-axes are obtained by calculating that of three phases along with the qd-axes where q-axis lags a-axis by  $\theta_r$ .

The stator currents in fictitious qd-axes are calculated by (4), where the transformation matrix given by (5).

$$\begin{bmatrix} i_{qs} \\ i_{ds} \\ i_0 \end{bmatrix} = [T] \begin{bmatrix} i_{as} \\ i_{bs} \\ i_{cs} \end{bmatrix} \quad (4)$$

$$T = \frac{2}{3} \begin{bmatrix} \cos\omega_r t & \cos(\omega_r t - \frac{2\pi}{3}) & \cos(\omega_r t + \frac{2\pi}{3}) \\ \sin\omega_r t & \sin(\omega_r t - \frac{2\pi}{3}) & \sin(\omega_r t + \frac{2\pi}{3}) \\ \frac{1}{2} & \frac{1}{2} & \frac{1}{2} \end{bmatrix} \quad (5)$$

It is noted that the zero sequence current,  $i_0$ , does not have any contribution to the resultant magnetic field. Three-phase current from two-phase stator currents are obtained with the help of inverse transformation matrix as:

$$\begin{bmatrix} i_{as} \\ i_{bs} \\ i_{cs} \end{bmatrix} = [T]^{-1} \begin{bmatrix} i_{qs} \\ i_{ds} \\ i_0 \end{bmatrix} \quad (6)$$

where:

$$[T]^{-1} = \begin{bmatrix} \cos\omega_r t & \sin\omega_r t & 1 \\ \cos(\omega_r t - \frac{2\pi}{3}) & \sin(\omega_r t - \frac{2\pi}{3}) & 1 \\ \cos(\omega_r t + \frac{2\pi}{3}) & \sin(\omega_r t + \frac{2\pi}{3}) & 1 \end{bmatrix} \quad (7)$$

Similarly, q- and d-axes voltages in stator frame may be calculated by (8).

$$\begin{bmatrix} v_{qs} \\ v_{ds} \end{bmatrix} = [T] \begin{bmatrix} v_{as} \\ v_{bs} \\ v_{cs} \end{bmatrix} \quad (8)$$

The relation between stationary current of q- and d-axes and rotor reference frame current rotating at an electrical speed  $\omega_r$  is given by (9).

$$\begin{bmatrix} i_{qs}^r \\ i_{ds}^r \end{bmatrix} = \begin{bmatrix} \cos\theta_r & -\sin\theta_r \\ \sin\theta_r & \cos\theta_r \end{bmatrix} \begin{bmatrix} i_{qs} \\ i_{ds} \end{bmatrix} \quad (9)$$

Similarly, the relation between stationary q- and d-axis voltage and reference voltage in rotor that is rotating at an electrical speed  $\omega_r$  is given by (10).

$$\begin{bmatrix} v_{qs}^r \\ v_{ds}^r \end{bmatrix} = \begin{bmatrix} \cos\theta_r & -\sin\theta_r \\ \sin\theta_r & \cos\theta_r \end{bmatrix} \begin{bmatrix} v_{qs} \\ v_{ds} \end{bmatrix} \quad (10)$$

The PMSM equivalent circuit can be obtained by using stator equations and is depicted in Figure 2.



Figure 2. PMSM equivalent circuit without core loss (a) q-axis circuit and (b) d-axis circuit

The voltages developed in rotor reference neglecting the core losses can be derived as in [7] and given by:

$$v_{qs}^r = R_s i_{qs}^r + L_q \frac{di_{qs}^r}{dt} + \omega_r L_d i_{ds}^r + \omega_r \lambda_{af} \quad (11)$$

$$v_{ds}^r = R_s i_{ds}^r + L_d \frac{di_{ds}^r}{dt} - \omega_r L_q i_{qs}^r \quad (12)$$

where,  $\omega_r \lambda_{af}$  is back emf;  $v_{qs}^r$  and  $v_{ds}^r$  are the stator voltages, and  $i_{qs}^r$  and  $i_{ds}^r$  are the stator currents in q- and d-axes, respectively, in rotor reference frame;  $R_s$  is the stator winding resistance;  $L_q$  and  $L_d$  are the q and, d-axis inductance of the stator winding with respect to rotor position; and  $\lambda_{af}$  is flux resulted from linking of rotor magnets and stator.

Inserting the values of stator current from (1) to (3) in (4), with respect to rotor reference, the stator currents can be obtained as (13).

$$\begin{bmatrix} i_{qs}^r \\ i_{ds}^r \end{bmatrix} = i_s \begin{bmatrix} \sin\delta \\ \cos\delta \end{bmatrix} = \begin{bmatrix} i_T \\ i_f \end{bmatrix} \quad (13)$$

From (13) it is obvious that stator current has two components,  $i_f$  and  $i_T$ , along d-and q-axis, respectively. Among them, only  $i_f$  has the contribution for producing field flux, because rest of the flux is supplied by the rotor magnets and can be considered as the equivalent source of current. Another component of these currents,  $i_T$ , that develops torque resulting from the linkage with rotor flux may also be called as torque producing component of currents. The angular speed of the rotor w.r.t. stator reference can be obtained as (14).

$$\dot{\theta} = \omega_r \quad (14)$$

The rotor position as well as speed define the mechanical dynamics of a machine that are deduced by the electromagnetic torque. This torque is calculated from the matrix of the machine considering other

important parameters, such as mechanical power, copper loss, magnetic energy storage. Besides, it is fact that there is no resulting power component for reference and in steady state condition the change in stored magnetic energy will be equal to zero. Therefore, the power output only be the difference among the input power and copper losses in steady state condition. The equation for input voltage of the PMSM is given by (15).

$$\mathbf{V} = \mathbf{R}i + \mathbf{L} \frac{di}{dt} + \mathbf{G}\omega_r i \quad (15)$$

The equation for instantaneous input power can be expressed as:

$$P_i = i^t \mathbf{V} = i^t \mathbf{R}i + i^t \mathbf{L} p i + i^t \mathbf{G}\omega_r i \quad (16)$$

where,  $i^t \mathbf{R}i$  and  $i^t \mathbf{L} \frac{di}{dt}$  depict the copper loss and stored magnetic energy, respectively. The remaining component of power is developed in the air-gap and denoted by the term  $i^t \mathbf{G}\omega_r i$  that is associated with speed of the rotor and known as air-gap power. Therefore, this air-gap power can also be calculated from the input power, the product of q-and d-axis stator current and voltage. For a symmetrical 3- $\phi$  system there is no zero sequence current, and hence power responsible for this current will be zero, hence input power can then be expressed by (17).

$$P_i = \frac{3}{2} [v_{qs}^r i_{qs}^r + v_{ds}^r i_{ds}^r] \quad (17)$$

Three-phase power is derived from two-phase (qd) PMSM. So, for power equivalence, the factor 3/2 is multiplied. Using the value of d-and q-axis voltage and current, the input power will be:

$$\begin{aligned} P_i = & \frac{3}{2} [R_s [(i_{qs}^r)^2 + (i_{ds}^r)^2] + \{L_q i_{qs}^r p i_{qs}^r + L_d i_{ds}^r p i_{ds}^r\} \\ & + \omega_r \{\lambda_{af} + (L_d - L_q) i_{ds}^r\} i_{qs}^r] \end{aligned} \quad (18)$$

the third term of (18) is the desired power from air-gap and this is also equal the product of speed of rotor in radian/second and  $T_e$  is electromagnetic torque . The equation for electromagnetic torque is then calculated as:

$$\begin{aligned} \omega_m T_e = P_a = & \frac{3}{2} \omega_r [\lambda_{af} + (L_d - L_q) i_{ds}^r] i_{qs}^r \\ \Rightarrow T_e = & \frac{3}{2} \frac{P}{2} [\lambda_{af} + (L_d - L_q) i_{ds}^r] i_{qs}^r \end{aligned} \quad (19)$$

where,  $\omega_m = 2\omega_r/P$  is mechanical speed in rad/s, and  $P$  indicates the pole numbers. Using the values of q-and d-axis currents from (13), by using the  $i_s$  and  $\delta$ , the  $T_e$  can be obtained as:

$$T_e = \frac{3P}{4} [\lambda_{af} i_s \sin \delta + \frac{1}{2} (L_d - L_q) i_s^2 \sin 2\delta] \quad (20)$$

The first part of (20) is obviously the synchronous torque that is developed due to the linkage of permanent magnetic field to the stator current. The remaining part clearly depicts the torque produced from the variation of the reluctance and hence also known as reluctance torque. The important fact from this equation is control variables are magnitude of  $i_s$  and  $\delta$  while rotor flux linkage and machine inductance are being constant. Meanwhile, including load fluctuations and parameter uncertainty the electromechanical dynamic motion equation for PMSM is:

$$T_e = J \frac{d\omega_m}{dt} + T_l + B\omega_m \quad (21)$$

where,  $\omega_m$ ,  $J$ , and  $B$  are the mechanical speed of the rotor, combined inertia of load and machine, and friction coefficient respectively.

### 3. STRUCTURE OF CONTROLLER

The combined control structure discussed in this paper is shown in Figure 3. To obtain a speed-control system of PMSM drives, a outer feedback is used to the core torque-control system, also known as vector

controller, in addition with RBFNN and PI controller. The measured speed  $\omega_r$  is used as the input to RBFNN to nullify the error between measured and reference speeds . The error speed, resulted from the difference of reference and RBFNN estimated speed, is passed through the conventional PI controller that produce reference electromagnetic torque  $T_e^*$ , for the vector controller and the change in torque inside the machine is used to minimize the speed error. If the error in speed is increased or decreased, the torque increases and decreases, respectively.

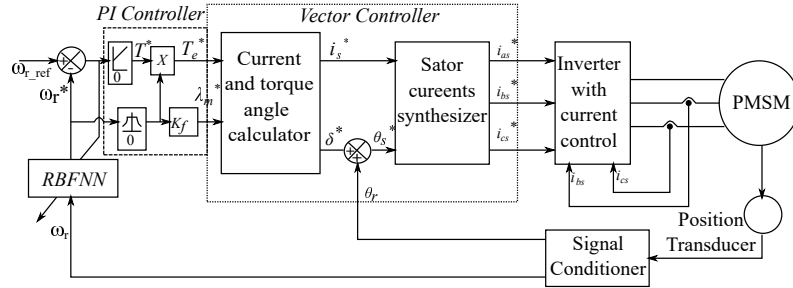


Figure 3. Overall control diagram

**3.1. RBFNN controller**

A 1 : 5 : 1 structured RBFNN, shown in Figure 4 is used for controlling the speed of PMSM and hence the overall control diagram is depicted in Figure 3. The output of the RBF controller is:

$$\omega_r^*(k) = \sum_{j=1}^m h_j(k)\psi_j(k) + b(k) \tag{22}$$

where  $m$  is the hidden layer neural nets,  $\psi_j$  is the weight value of net  $j$ ,  $h_j$  is the Gaussian function output. In RBF, the measured speed,  $\omega_r$  is used as input, and  $\mathbf{h} = [h_1, \dots, h_m]$ , and  $h_j$  is derived from a set of basis function given by:

$$h_j = \exp\left(-\frac{\|\omega_r - c_j\|^2}{2\zeta^2}\right) \tag{23}$$

where  $j = 1, \dots, m$ .  $b_j > 0$ ,  $\mathbf{c}_j = [c_{j1}, \dots, c_{jn}, \dots, c_{jm}]$  and  $\zeta$  is the variance that modulate the region of similarity and the weight vector,  $\Psi = [\psi_1, \psi_2, \dots, \psi_j]^T$ . The the tracking error is given by:

$$\omega_{error}(k) = \omega_{r\_ref}(k) - \omega_r^*(k) \tag{24}$$

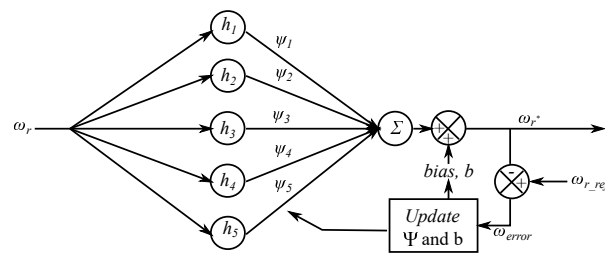


Figure 4. RBFNN controller

The cost function used here is given by (25).

$$E(k) = \frac{1}{2} \omega_{error}(k)^2 \tag{25}$$

The learning algorithm based on steepest descent method is written as:

$$\Delta\psi_j(k) = -\gamma \frac{\delta E(k)}{\delta \psi} = \gamma \omega_{error}(k) \frac{\delta \omega_r^*(k)}{\delta u(k)} h_j \tag{26}$$

$$\psi_j(k) = \psi_j(k-1) + \Delta\psi_j(k) + \epsilon \Delta\psi_j(k) \tag{27}$$

where,  $\gamma$  is learning rate,  $\epsilon$  is momentum factor,  $\gamma \in [0, 1]$ , and  $\epsilon \in [0, 1]$ . For the same reason, we can get:

$$\Delta\zeta_j(k) = -\gamma \frac{\delta E(k)}{\delta \zeta_j} = \gamma \omega_{error}(k) \frac{\delta \omega_r^*(k)}{\delta u(k)} \frac{\delta u(k)}{\delta \zeta_j} = \gamma \omega_{error}(k) \frac{\delta \omega_r^*}{\delta u(k)} \psi_j h_j \frac{|\omega_r - c_{ij}|^2}{\zeta_j^3} \quad (28)$$

$$\zeta_j(k) = \zeta_j(k-1) + \gamma \Delta\zeta_j(k) + \epsilon(\zeta_j(k-1) - \zeta_j(k-2)) \quad (29)$$

where,  $\frac{\delta y(k)}{\delta u(k)}$  is *Jacobian*, that gives the sensitivity of the system. *Jacobian* value can be derived from the the sign of  $\frac{\delta y(k)}{\delta u(k)}$ .

$$\Delta c_{ij}(k) = -\gamma \frac{\delta E(k)}{\delta c_{ij}} = \gamma \omega_{error}(k) \frac{\delta \omega_r^*(k)}{\delta u(k)} \frac{\delta u(k)}{\delta c_{ij}} = \gamma \epsilon c(k) \frac{\delta \omega_r^*(k)}{\delta u(k)} \psi_j h_j \frac{\omega_{ri} - c_{ij}}{\zeta_j^2} \quad (30)$$

$$c_{ij}(k) = c_{ij}(k-1) + \gamma \Delta c_{ij}(k) + \epsilon(c_{ij}(k-1) - c_{ij}(k-2)) \quad (31)$$

#### 4. RESULTS AND DISCUSSION

To validate the proposed algorithm, several computer simulations were performed in Matlab, and for simplicity following assumptions are taken into consideration: (i) magnetic circuit saturation is neglected, (ii) eddy current as well as hysteresis current losses are not regarded, and (iii) sinusoidal magnetic field is considered. Moreover, the inertia constant and friction coefficients,  $J$  and  $B$ , respectively are considered as uncertain. The uncertain may include discrepant in production, complex working environment, change in temperature and mechanical wear as well. The vector control of PMSM is analogous to that for induction motors. This method splits the torque and flux channels exploiting its stator excitation inputs. In this section, the proposed control method applied to PMSM is simulated by using MATLAB environment to verify the performance. In the simulations, the important machine parameters used are listed in Table 1.

Table 1. Parameters for simulations

Machine parameters	Value
Resistance of stator winding	1.4
Number of poles	6
Inertia constant, J	0.0012
Friction constant, B	0.01
d-axis inductance	0.0056
q-axis inductance	0.009
Rotor flux in Wb	0.1546

To present a clear picture for the algorithm and steps of simulations, it is necessary to mention all the variables and/or parameters. Besides, the parameters above mentioned in Table 1, the other parameters are as follows: DC link voltage,  $v_{dc} = 285$  V, reference speed,  $\omega_{ref} = 400$  rad/sec, PWM switching frequency,  $f_s = 20$  kHz, base torque,  $T_b = 5.5631$  N-m, base current,  $I_b = 12$  A, base speed,  $\omega_b = 628.6$  rad/sec, base voltage,  $V_b = 97.138$  V, d-axis current,  $i_{f_{ref}} = -1e^{-16}$  A, load torque,  $T_l = 0.25 * T_b$  N-m. The potential performance for the offered speed control method is illustrated by the computer simulations obtained from both constant and variable speeds. The steps for simulation using Matlab code is presented in Algorithm 1. Firstly, the constant speed of 400 rad/sec is considered as the target speed of the machine shown in Figure 5, and then a variable step of speed shown in Figure 6 is used to observe the accuracy of the control system. The proposed control method is RBFNN based PI controller. For the performance comparison, PI based vector control algorithm is applied first and then RBFNN is superimposed. The speed and torque performances of the PMSM are observed with and without the application of RBFNN. In this case the RBFNN is a memoryless adaptation scheme since the algorithm neither use the past sample nor retain the previous adaptation direction. Hence the observations are used only once, extra memory is not required for storing trained samples. To perform the simulation using RBFNN, the used values of the parameters were the mean value,  $c = \omega_{ref} * [-3, -2, -1, 1, 2]$ , the variance,  $\zeta = 2$ , the learning rate of 0.001, random bias,  $b$ , and five random variable values for initial weight vector,  $\psi$ .

**Algorithm 1** Simulation steps and procedure for speed control of PMSM using RBFNN

---

```

1: System Initialize with  $dt = 1e^{-6}$ ,  $t_f = 0.1$ ,  $m = 1$ ,  $z = 1$ ,  $K_{pi} = 10$ ,  $K_p = 2$ ,  $K_i = 1$ 
2: while ( $t < t_f$ ) do
3:   Define variable speed if necessary
4:   Speed error  $\omega_{err} = \omega_{ref} - \omega_r$ 
5:   Speed PI controller  $y = y + \omega_{err} * dt$ 
6:   Torque limiter,  $T_{eref} = K_p * \omega_{err} + K_i * y$ 
7:   if  $T_{eref} > 2 * T_b$ ,  $T_{eref} = 2 * T_b$  then
8:     else
9:       if  $T_{eref} < -2 * T_b$ ,  $T_{eref} = -2 * T_b$  then
10:    Calculate  $it_{ref}$  using (19) and  $is_{ref}$  using (13)
11:    if  $it_{ref} \geq 0$ ,  $\delta_{ref} = \pi/2$  then
12:      else
13:        if  $it_{ref} < 0$ ,  $\delta_{ref} = -\pi/2$  then
14:        Calculate phase current using (1-3)
15:        Generate PWM signal
16:        if  $uax = K_{pi} * (ias_{ref} - ias) > 0$ ,  $uax = 1$  then ▷ Repeat for b and c phases
17:        else
18:          if  $uax < -1$ ,  $uax = -1$  then
19:          if  $t_s > 1/f_s$  then
20:             $uax1 = uax$ ,  $ubx1 = ubx$ ,  $ucx1 = ucx$ ,  $t_s = 0$ 
21:            if  $uax1 \geq ramps$ ,  $vao = vdc/2$  then ▷ Repeat for b and c phases
22:            else
23:              if  $uax1 < ramps$ ,  $vao = -vdc/2$  then ▷ Repeat for b and c phases
24:            Compute voltages  $vab = vao - vbo$  and  $vas = (vab - vca)/3$ 
25:            Compute  $v_{qs}$  and  $v_{ds}$  using (8)
26:            Calculate  $di_{qs}^r$  and  $di_{ds}^r$  using Eq.(11-12)
27:            Update  $i_{qs}$  and  $i_{ds}$ , then obtain  $i_s = \sqrt{i_{qs}^2 + i_{ds}^2}$ 
28:            Calculate torque angle using (13) and torque using (19)
29:            Obtain differential speed  $d\omega$  from (21)
30:            Update speed  $\omega_r = \omega_r + d\omega$  ▷ Reference speed to RBFNN
31:            for  $i \leftarrow 0 : length(c)$  do
32:               $h_i = exp\left(-\frac{\|\omega_r - c_i\|^2}{2\zeta^2}\right)$ 
33:            RBFNN output speed  $\omega_r^* = \psi * h' + b$ 
34:            Speed error  $w_{err} = w_{ref} - \omega_r^*$ 
35:            Update  $\psi$  using (27) and  $c$  using (31)
36:            Calculate  $d\theta_r$  using (14) and update  $\theta_r$ 
37:            Calculate Phase current using (6)
38:            Define ramps =  $sign*(2/(1/(2*f_c)))*dt+ramps$ 
39:            if  $ramps > 1$ ,  $sign = -1$  then
40:              else
41:                if  $ramps < -1$ ,  $sign = 1$  then
42:                 $t = t + dt$ ,  $t_s = t_s + dt$ 
43:                if  $z > 16$  then
44:                  count t
45:                   $\omega_{rm}(m) = \omega_r/\omega_b$ 
46:                   $m = m + 1$ ,  $z = 1$ 
47:                 $z = z + 1$ 
return  $\omega_{rm}$ 

```

---



The Figure 5(a) depicts the speed tracing process of the system using PI based vector control method with and without RBFNN. The dashed line (-) represents the target speed, the dash-dotted line(-.-) depicts the simulated speed without RBFNN and the solid line(-) indicates the tracing speed by using the proposed RBFNN based PI controller. The motor is in rest at the beginning due to motor inertia and PI based vector control method traces the target speed linearly where the settle time is around 0.0189 second whereas if RBFNN is applied, there is a transient in tracing the reference speed. The time required to cope up with the target speed is around 0.006 second. Though, it is apparent that the without RBFNN, the method traces the target speed but there is an obvious difference between target and estimated speed that is figured out in the zoom section in Figure 5(a). On the other hand, in the zoom view it is observed that the proposed algorithm perfectly estimated the reference speed. The effect of this speed tracking is observed in the torque performance of the machine shown in Figure 5(b). Without RBFNN, the machine maintains its predefined threshold torque until the rotor reaches the reference speed and even after that there still a considerable amount constant torque is available due to the difference between target and estimated speed. This problem is solved by using RBFNN and the residual torque is minimized.

At the same time, the reference phase current shows a fluctuation during the speed mismatch at the beginning and for simplicity the curves for phase current obtained from the offered method is illustrated in Figure 5(c). The phase currents resume normal values after the motor running at the steady state speed for the application of proposed method. The the d-q axes currents are presented in Figure 5(d) during the proposed method of speed control, the contribution of d-axis current is zero as shown in Figure 5(d) and hence in this case electromagnetic torque  $T_e$  become proportional to  $i_q$ , refer to equation (19), which is similar for DC motor with independent field excitation. From the dq-axes current it is obvious that at starting q-axis current increases and then fluctuate around a small positive current due to stator resistance.

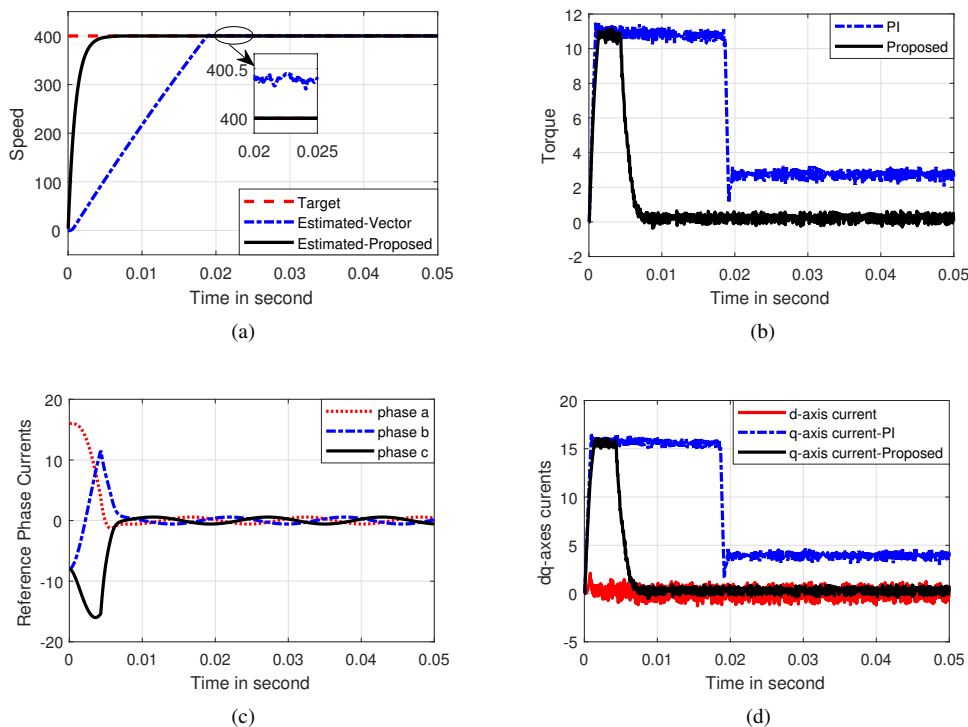


Figure 5. Performance measurements (a) speed, (b) torque response, (c) reference phase currents, and (d) d-q axes currents

To uphold the precision of the suggested method for the multiple ramps in speed, variable speed is used as a target speed. In this case, three reference speeds are used, from 400 to 500 and then to 300 rad/sec as shown in Figure 6(a). The curves from simulations depict that the presented control method outcompetes the existing PI based vector control system and RBFNN based method estimates the speed very fast as well

as precisely even there is a step change in speed. Likewise, the torque reduces to its normal value when the rotor speed traces the command speed to equalize the load and friction torque as shown in Figure 6(b). So, in a nutshell, it can be said that the proposed RBFNN based PI vector control system for controlling the speed of PMSM exhibits remarkable stability of the system as well as persistent in performance for a large speed range.

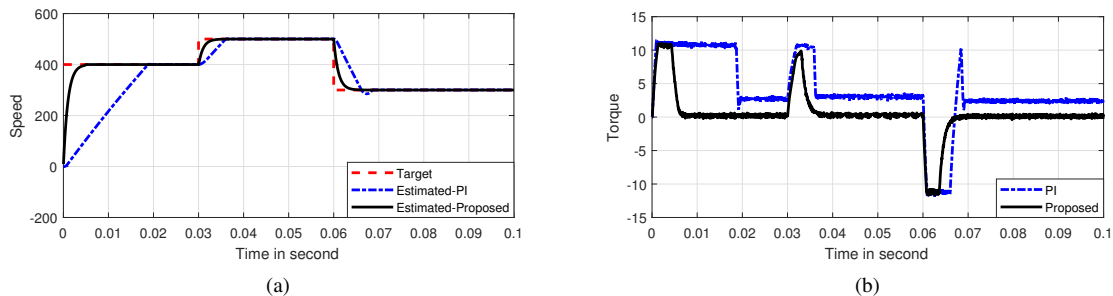


Figure 6. Performance measurements for different speed target (a) response to a ramp in speed and (b) developed torque for different speeds

## 5. CONCLUSION

The inertia uncertainty and the friction coefficient result deficient system steadiness and substantial swing in speed of PMSM. By this research, a robust speed controlling algorithm is investigated and implemented in Matlab simulation environment. Firstly, considering the uncertainty parameters and variation of load, dynamic system equations of PMSM is derived. Then, a memoryless RBFNN-based PI speed controller for PMSM drives is proposed that is easy to implement but robust against speed fluctuations. For auto adjustment of control gain in PI, the control law for RBFNN is proposed by using the gradient decent algorithm to achieve an adequate system stability, and powerful anti-swing performance within the defined speed span. Simulation results for different speeds depict that the RBFNN based PI controller successfully track the new speed very fast whereas, only PI controller slowly follow the target speed and can not perfectly reach the target speed. Therefore, the suggested control method provide guarantee of the accurate as well as fast tracking of speed. This presented method may be exploited to different control system having complex load disturbances and parameter uncertainty.




## REFERENCES

- [1] P. C. Krause, O. Wasynczuk, S. D. Sudhoff, and S. D. Pekarek, *Analysis of electric machinery and drive systems*, New York, NY, USA: Wiley, 2013.
- [2] J. Wu, J. Zhang, B. Nie, Y. Liu, and X. He, "Adaptive control of PMSM servo system for steering-by-wire system with disturbances observation," in *IEEE Transactions on Transportation Electrification*, vol. 8, no. 2, pp. 2015-2028, Jun. 2022, doi: 10.1109/TTE.2021.3128429.
- [3] S. Murshid and B. Singh, "Implementation of PMSM drive for a solar water pumping system," in *IEEE Transactions on Industry Applications*, vol. 55, no. 5, pp. 4956-4964, Sept.-Oct. 2019, doi: 10.1109/TIA.2019.2924401.
- [4] C. Elmas and O. Ustun, "A hybrid controller for the speed control of a permanent magnet synchronous motor drive," *Control Engineering Practice*, vol. 16, no. 3, pp. 260-270, 2008, doi: 10.1016/j.conengprac.2007.04.016.
- [5] Y. S. Kung, N. P. Thanh, and H. H. Chou, "Design and implementation of a microprocessor-based PI controller for PMSM drives," *Applied Mechanics and Materials*, vol. 764-765, pp. 496-500, 2015, doi: 10.4028/www.scientific.net/AMM.764-765.496.
- [6] J. -W. Jung, Y. -S. Choi, V. Q. Leu, and H. H. Choi, "Fuzzy PI-type current controllers for permanent magnet synchronous motors," *IET Electric Power Applications*, vol. 5, no. 1, pp. 143-152, 2011, doi: 10.1049/iet-epa.2010.0036.
- [7] J. -W. Jung, V. Q. Leu, T. D. Do, E. -K. Kim, and H. H. Choi, "Adaptive PID speed control design for permanent magnet synchronous motor drives," in *IEEE Transactions on Power Electronics*, vol. 30, no. 2, pp. 900-908, Feb. 2015, doi: 10.1109/TPEL.2014.2311462.
- [8] K. Suman and A. T. Mathew, "Speed control of permanent magnet synchronous motor drive system using PI, PID, SMC and SMC plus PID controller," *2018 International Conference on Advances in Computing, Communications and Informatics (ICACCI)*, 2018, pp. 543-549, doi: 10.1109/ICACCI.2018.8554788.
- [9] X. Gao, M. Abdelrahman, C. M. Hackl, Z. Zhang, and R. Kennel, "Direct predictive speed control with a sliding manifold term for PMSM drives," in *IEEE Journal of Emerging and Selected Topics in Power Electronics*, vol. 8, no. 2, pp. 1258-1267, Jun. 2020, doi: 10.1109/JESTPE.2019.2923285.
- [10] L. Feng, M. Deng, S. Xu, and D. Huang, "Speed regulation for PMSM drives based on a novel sliding mode controller," in *IEEE Access*, vol. 8, pp. 63577-63584, 2020, doi: 10.1109/ACCESS.2020.2983898.




- [11] Q. Wang, H. Yu, M. Wang, and X. Qi, "An improved sliding mode control using disturbance torque observer for permanent magnet synchronous motor," in *IEEE Access*, vol. 7, pp. 36691-36701, 2019, doi: 10.1109/ACCESS.2019.2903439.
- [12] W. Xu, Y. Jiang, and C. Mu, "Novel composite sliding mode control for PMSM drive system based on disturbance observer," in *IEEE Transactions on Applied Superconductivity*, vol. 26, no. 7, pp. 1-5, Oct. 2016, doi: 10.1109/TASC.2016.2611623.
- [13] K. Paponpen and M. Konghirun, "An improved sliding mode observer for speed sensorless vector control drive of PMSM," *2006 CES/IEEE 5th International Power Electronics and Motion Control Conference*, 2006, pp. 1-5, doi: 10.1109/IPEMC.2006.4778137.
- [14] I.-C. Baik, K.-H. Kim, and M.-J. Youn, "Robust nonlinear speed control of PM synchronous motor using boundary layer integral sliding mode control technique," in *IEEE Transactions on Control Systems Technology*, vol. 8, no. 1, pp. 47-54, Jan. 2000, doi: 10.1109/87.817691.
- [15] A. Brosch, O. Wallscheid, and J. Bocker, "Model predictive control of permanent magnet synchronous motors in the over-modulation region including six-step operation," in *IEEE Open Journal of Industry Applications*, vol. 2, pp. 47-63, 2021, doi: 10.1109/OJIA.2021.3066105.
- [16] S. Walz and M. Liserre, "Hysteresis model predictive current control for PMSM with LC filter considering different error shapes," in *IEEE Open Journal of Power Electronics*, vol. 1, pp. 190-197, 2020, doi: 10.1109/OJPEL.2020.3000466.
- [17] C. Xue, L. Ding, and Y. R. Li, "Model predictive control with reduced common-mode current for transformerless current-source PMSM drives," in *IEEE Transactions on Power Electronics*, vol. 36, no. 7, pp. 8114-8127, Jul. 2021, doi: 10.1109/TPEL.2020.3045652.
- [18] M. Liu, K. W. Chan, J. Hu, W. Xu, and J. Rodriguez, "Model predictive direct speed control with torque oscillation reduction for PMSM drives," in *IEEE Transactions on Industrial Informatics*, vol. 15, no. 9, pp. 4944-4956, Sep. 2019, doi: 10.1109/TII.2019.2898004.
- [19] A. Mora, Á. Orellana, J. Juliet, and R. Cárdenas, "Model predictive torque control for torque ripple compensation in variable-speed PMSMs," in *IEEE Transactions on Industrial Electronics*, vol. 63, no. 7, pp. 4584-4592, Jul. 2016, doi: 10.1109/TIE.2016.2536586.
- [20] T.-S. Lee, C.-H. Lin, and F.-J. Lin, "An adaptive  $H_\infty$  controller design for permanent magnet synchronous motor drives," *Control Engineering Practice*, vol. 13, no. 4, pp. 425-439, 2005, doi: 10.1016/j.conengprac.2004.04.001.
- [21] K.-Y. Cheng and Y.-Y. Tzou, "Fuzzy optimization techniques applied to the design of a digital PMSM servo drive," in *IEEE Transactions on Power Electronics*, vol. 19, no. 4, pp. 1085-1099, Jul. 2004, doi: 10.1109/TPEL.2004.830036.
- [22] R. Kumar, R. A. Gupta, and A. K. Bansal, "Identification and control of PMSM using artificial neural network," *2007 IEEE International Symposium on Industrial Electronics*, 2007, pp. 30-35, doi: 10.1109/ISIE.2007.4374567.
- [23] S. Brock, J. Deskur, and K. Zawirski, "Robust speed and position control of PMSM," *ISIE '99. Proceedings of the IEEE International Symposium on Industrial Electronics (Cat. No.99TH8465)*, 1999, vol. 2, pp. 667-672, doi: 10.1109/ISIE.1999.798692.
- [24] M. Kaminski, "Nature-inspired algorithm implemented for stable radial basis function neural controller of electric drive with induction motor," *Energies*, vol. 13, no. 24, p. 6541, 2020, doi: 10.3390/en13246541.
- [25] R. Wang, D. Li, and K. Miao, "Optimized radial basis function neural network based intelligent control algorithm of unmanned surface vehicles," *Journal of Marine Science and Engineering*, vol. 8, no. 3, p. 210, 2020, doi: 10.3390/jmse8030210.
- [26] S. Slema, A. Errachdi, and M. Benrejeb, "A radial basis function neural network model reference adaptive controller for non-linear systems," *2018 15th International Multi-Conference on Systems, Signals & Devices (SSD)*, 2018, pp. 958-964, doi: 10.1109/SSD.2018.8570538.
- [27] H. Chaoui, M. Khayamy, and O. Okoye, "Adaptive RBF network based direct voltage control for interior PMSM based vehicles," in *IEEE Transactions on Vehicular Technology*, vol. 67, no. 7, pp. 5740-5749, Jul. 2018, doi: 10.1109/TVT.2018.2813666.
- [28] S. Li, J. Li, and Y. Shi, "An RBFNN-based direct inverse controller for PMSM with disturbances," *Complexity*, vol. 2018, 2018, doi: 10.1155/2018/4034320.

## BIOGRAPHIES OF AUTHORS



**Md. Alamgir Hossain**    is pursuing Ph.D. from the Department of Electrical and Electronic Engineering, Khulna University of Engineering & Technology (KUET), Bangladesh from where he obtained his Bachelor of Science in Electrical and Electronic Engineering Degree in 2007. He obtained Master of Engineering Degree from Osaka Prefecture University, Japan in 2012. His research interest includes artificial intelligence, machine learning, electrical drives systems, energy internet in microgrid. Further info is available on his homepage: <http://www.kuet.ac.bd/eee/alamgir>. He can be contacted at email: mah@eee.kuet.ac.bd.



**Md. Shahjahan**    received B.Sc. in Electrical and Electronic Engineering from Bangladesh Institute of Technology, M.Eng. and D.Eng. from University of Fukui, Japan, degree in 1996, 2003, and 2006, respectively. Presently he is a Professor of Electrical and Electronic Engineering department of Khulna University of Engineering and Technology, Bangladesh. His research interest are artificial neural network, machine learning, data mining, biomedical signal processing. He is a member of IEEE. He has published more than 80 international conference and reputed journal papers. Further info is available on his homepage: <http://www.kuet.ac.bd/eee/jahan>. He can be contacted at email: jahan@eee.kuet.ac.bd.